Available online at www.sciencedirect.com
SCIENCE DIRECT®
Journal of Computational Physics 214 (2006) 284–298
JOURNAL OF COMPUTATIONAL PHYSICS
www.elsevier.com/locate/jcp

Quasineutral particle simulation technique for whistlers ☆

Martin Lampe [a,*], Glenn Joyce [b], Wallace M. Manheimer [c], Anatoly Streltsov [c], Gurudas Ganguli [a]

[a] *Plasma Physics Division, Naval Research Laboratory, Washington, DC 20375-5346, United States*
[b] *George Mason University, Fairfax, VA, United States*
[c] *Icarus Research, Inc., Bethesda, MD, United States*

Received 3 March 2005; received in revised form 19 September 2005; accepted 21 September 2005
Available online 9 November 2005

Abstract

We present a new hybrid fluid/PIC simulation scheme for whistlers, which eliminates both the speed-of-light time scale and the electron plasma oscillation time scale, and concentrates simulation resources on the resonant parts of electron phase space that control whistler evolution. The code runs with time steps on the order of the electron gyrofrequency, with extremely accurate energy conservation and numerical stability. Examples are shown of application to whistler instability growth and saturation, and ducting of whistlers in density channels.

Keywords: Plasma simulation; Particle simulation; Particle-in-cell simulation; Whistlers; Magnetospheric plasma

1. Introduction

Whistlers [1,2] are right-hand polarized electromagnetic waves that are carried by the electrons in a plasma, with frequency in the range below the electron cyclotron frequency $\Omega \equiv eB_0/mc$ but above the lower-hybrid frequency. Here, B_0 is the ambient magnetic field and m is the electron mass. Whistlers are slow waves, i.e., the phase velocity $\omega/k \ll c$, and therefore the source for the wave magnetic field is overwhelmingly the electron current, rather than the displacement current. Furthermore, in situations of interest the electron plasma frequency $\omega_p \equiv (4\pi n_0 e^2/m)^{1/2}$ is typically much larger than Ω, and thus certainly very large compared to ω. Here n_0 is the ambient electron density. The waves are thus quasineutral, i.e., wave perturbations $n - n_0$ are small compared to n_0 itself, even if the wave amplitude is large. (It is important to note that this does not mean that the electrostatic field is negligible; a small perturbation to n can lead to a very large electrostatic field. Ion

☆ Supported by Office of Naval Research.
* Corresponding author. Tel.: +1 202 767 4041; fax: +1 202 767 1607.
E-mail address: lampe@nrl.navy.mil (M. Lampe).

0021-9991/$ - see front matter © 2005 Elsevier Inc. All rights reserved.
doi:10.1016/j.jcp.2005.09.015

sound waves, for example, are in essence quasineutral electrostatic waves.) Numerical simulation schemes involving the use of a straightforward electromagnetic field solver are thus extremely inefficient, since the time steps must be small enough to resolve the Courant condition for speed c, and must also be small enough to resolve the plasma frequency time scale. Both of these time scales are much smaller than the wave period. In addition, *particle simulation* schemes based on a full electromagnetic field solver are particularly susceptible to noise, since the charge density $\rho(\mathbf{x},t) \equiv -e[n(\mathbf{x},t) - n_0(\mathbf{x})]$ is obtained from small perturbations to the finite number of simulation particles in a given region, and the electrostatic component of the electric field in essence derives from $\rho(\mathbf{x},t)$ through Poisson's equation.

Traditionally, the Darwin model [3] has been used to address these issues that arise in numerical simulation of slow electromagnetic waves. In this approach, the *solenoidal* component of the displacement current (i.e., essentially the transverse component, for a linear plane wave) is neglected in Maxwell's equations. The *irrotational* component of the displacement current cannot be neglected, since it is essentially the time derivative of the electrostatic field, i.e., the longitudinal electric field in a linear plane wave. The separation of the solenoidal component of the displacement current is difficult, and it enormously complicates the algorithmic schemes as well as significantly increasing the running time of Darwin codes. Quasineutrality is a separate issue that has also been addressed within the Darwin scheme [3,4], but it leads to additional complications.

Another approach which has been used [5,6] to study the nonlinear evolution of whistlers is to begin with equations relating the slowly varying quantities ψ and α that characterize the long-time evolution of resonant electrons. Here, ψ is the difference in phase between the gyro motion of an electron and the magnetic field of the wave, and α is the pitch angle of the electron. This approach permits the use of long-time steps, but it can only be used for the case of a single discrete wave, as the definition of ψ inherently depends on there being well-defined (but possibly slowly varying) values of k and ω for the wave.

In the present paper, we present a new, efficient and simple approach which is not restricted to the case of a single mode, and which takes advantage of the characteristics of whistlers (and other low-frequency electromagnetic waves). Specifically, a whistler is carried primarily by the large number of cool non-resonant electrons, and it is quite accurate to represent these electrons as a cold fluid [1,2]. However, the whistler may be damped, or driven unstable, by a smaller class of fast electrons that are in cyclotron resonance with the wave. These electrons also engage in complex nonlinear behaviors such as trapping and stochastic diffusion that control the evolution of large-amplitude waves and can result in nonlinear effects such as instability saturation and triggered emission. In our hybrid scheme, the energetic electrons of interest are followed using the particle-in-cell (PIC) technique, while the bulk of the electrons are represented as a cold fluid, which can be advanced numerically orders of magnitude faster. Because of the presence of the cold fluid, we are able, within a fully self-consistent scheme, to eliminate the *entire* displacement current from Maxwell's equations (not just the solenoidal part), and to determine the electrostatic field directly from the requirement of quasineutrality, rather than by requiring that Poisson's equation be satisfied. Speed-of-light phenomena cannot occur since there is no displacement current, and electron plasma oscillations cannot occur since quasineutrality is enforced. It is therefore not necessary to resolve the ω_p time scale. The result is a code which we call HEMPIC (hybrid electromagnetic PIC) that runs with time steps typically $\sim 1/4\Omega$. At present we are running a 2-D Cartesian version of HEMPIC, but there is no reason why the scheme cannot be 2-D cylindrical or fully 3-D. Also at present, HEMPIC follows only the motion of electrons and treats the ions as an immobile neutralizing background, but the approach could be extended to include ion kinetics, in order to study, e.g. ion cyclotron waves.

2. Basic equations: cold fluid only

To introduce the novel features of our scheme in the clearest way, we shall begin by discussing a simplified model in which the plasma is represented entirely as a cold electron fluid, with an immobile neutralizing ion background. We shall use the subscript c to denote cold-electron quantities. In a later section, we generalize the model to include PIC simulation electrons in addition to the cold electron fluid, and we shall then use the subscript p to denote particle-electron quantities.

Our starting point is Maxwell's equations, with the displacement current fully neglected:

$$\nabla \times \mathbf{E} = -\frac{1}{c}\frac{\partial \mathbf{B}}{\partial t}, \tag{1}$$

$$\nabla \times \mathbf{B} = -\frac{4\pi}{c} n_c e \mathbf{v}_c, \tag{2}$$

$$\nabla \cdot \mathbf{B} = 0, \tag{3}$$

where n_c and $\mathbf{v}_c$ are the cold-electron density and flow velocity. Because the displacement current has been neglected, Eq. (2) implies that the electron current be divergence-free,

$$\nabla \cdot (n_c \mathbf{v}_c) = 0. \tag{4}$$

It follows that if

$$n_c(\mathbf{x}, t) = n_0(\mathbf{x}) \tag{5}$$

at $t = 0$, then Eq. (5) will be satisfied at all times. Poisson's equation is not used; instead, the quasineutrality condition, i.e., Eq. (4) or Eq. (5) determines the electrostatic component of the electric field.

Using the fact that $n_0(\mathbf{x})$ is time-independent, and therefore also $n_c(\mathbf{x})$ is time-independent, Eqs. (1) and (2) can be reduced to a single equation relating $\mathbf{E}$ to the current $n_c e \mathbf{v}_c$,

$$\frac{\partial \mathbf{v}_c}{\partial t} = \frac{c^2}{4\pi n_c e} \nabla \times \nabla \times \mathbf{E}. \tag{6}$$

We use Eq. (6) to push the cold-fluid velocity $\mathbf{v}_c$ forward in time. Notice that this procedure guarantees that

$$\frac{\partial}{\partial t} \nabla \cdot (n_c \mathbf{v}_c) = 0, \tag{7}$$

so that if the quasineutrality condition (4) is satisfied at $t = 0$, it will continue to be satisfied at every time step. Notice also that it is the electromagnetic field equations that have been used to determine $\mathbf{v}_c$. We have not yet mentioned the electron fluid equations.

We use the cold-fluid momentum equation, written as

$$\frac{e\mathbf{E}}{m} = -\frac{\partial \mathbf{v}_c}{\partial t} - \mathbf{v}_c \cdot \nabla \mathbf{v}_c - \frac{e\mathbf{v}_c \times \mathbf{B}}{mc}, \tag{8}$$

to determine $\mathbf{E}$. However, the equation in this form is not suitable for use in a finite-difference code, because the $\partial v_c/\partial t$ term on the RHS leads to numerical instability. To avoid this problem, we use (6) to eliminate $\partial v_c/\partial t$ from (8). The resulting equation for $\mathbf{E}$ is

$$\nabla \times \nabla \times \mathbf{E} + \frac{\omega_{pc}^2}{c^2}\mathbf{E} = -\frac{4\pi n e}{c^2}\mathbf{v}_c \cdot \nabla \mathbf{v}_c - \frac{\omega_{pc}^2}{c^3}\mathbf{v}_c \times \mathbf{B}. \tag{9}$$

Eq. (9) is an elliptic partial differential equation that determines the complete vector $\mathbf{E}$, including both the solenoidal and irrotational parts. It is thus never necessary to calculate the charge density or to use Poisson's equation. Eq. (9) contains no time derivatives, and thus relates $\mathbf{E}$ to $\mathbf{v}$ and $\mathbf{B}$ at the same time, while Eq. (6) is a time-stepping equation that relates $\mathbf{E}$ at half time steps to $\mathbf{v}_c$ at whole time steps. Thus, the equations cannot be advanced in a fully time-centered finite-difference scheme. However, in Section 4, we show that a predictor–corrector–corrector solution procedure can be devised which is remarkably stable (fifth order in the time step) and highly accurate. When working in Cartesian coordinates with periodic boundary conditions, we use Fourier transform (FFT) to solve Eq. (9). In non-periodic systems we use successive over-relaxation. It is also possible to develop hybrid techniques that use FFT only for those coordinates that are periodic.

3. Linear plane waves in uniform media

Eqs. (2), (3), (6), and (9) may constitute an unfamiliar set of equations for determining $\mathbf{v}$, $\mathbf{E}$ and $\mathbf{B}$. Thus, it is perhaps useful to pause here to derive the linear whistler dispersion relation from these equations, in order to establish the relation between our approximations and those that are familiar from the linear theory of

whistlers. In addition, a linearized wave theory will be useful in the following section to guide us in the design of a stable and accurate finite-difference solution procedure. We assume here that n_0 and $\mathbf{B}_0$ are uniform, and that the perturbation consists of a small-amplitude wave of form $\exp(\mathrm{i}\mathbf{k}\cdot\mathbf{x} - \mathrm{i}\omega t)$. We choose coordinates (in this section only) so that $\mathbf{k}$ is in the x-direction, $\mathbf{B}_0$ lies in the x–y plane, and θ is the angle between $\mathbf{k}$ and $\mathbf{B}_0$. Then (4) implies that $\mathbf{k}\cdot\mathbf{v}_c = 0$, i.e., $\mathbf{v}_x = 0$. Neglecting nonlinear terms, Eqs. (6) and (9) then reduce to:

$$-\mathrm{i}\omega\mathbf{v}_c = -\frac{k^2c^2}{4\pi n_0 e}\hat{i}_x \times \hat{i}_x \times \mathbf{E}, \tag{10}$$

$$\mathbf{E} - \frac{k^2c^2}{\omega_{pc}^2}\hat{i}_x \times \hat{i}_x \times \mathbf{E} = \frac{\mathbf{B}_0 \times \mathbf{v}}{c}. \tag{11}$$

Noting that $\mathbf{B}_0$ has only x and y components, and $\mathbf{v}_c$ has only y and z components, Eq. (10) can be written as:

$$-\mathrm{i}\omega v_y = \frac{k^2c^2}{4\pi n_0 e}E_y, \tag{12a}$$

$$-\mathrm{i}\omega v_z = \frac{k^2c^2}{4\pi n_0 e}E_z, \tag{12b}$$

while Eq. (11) can be written as:

$$E_x = \frac{v_z}{c}B_0 \sin\theta, \tag{13a}$$

$$\left(1 + \frac{k^2c^2}{\omega_{pc}^2}\right)E_y = -\frac{v_z}{c}B_0\cos\theta, \tag{13b}$$

$$\left(1 + \frac{k^2c^2}{\omega_{pc}^2}\right)E_z = \frac{v_y}{c}B_0\cos\theta. \tag{13c}$$

Eqs. (12) and (13) yield a right-hand-polarized normal mode with dispersion relation

$$\omega = \frac{\Omega\cos\theta}{1 + \omega_{pc}^2/k^2c^2}. \tag{14}$$

There are no electron plasma oscillations contained within Eqs. (12) and (13).

The dispersion relation derived by Helliwell (Eq. (3.12) of [2]) under the "quasi-longitudinal approximation" is

$$\frac{k^2c^2}{\omega^2} = 1 + \frac{\omega_{pc}^2}{\omega(\Omega\cos\theta - \omega)}. \tag{15}$$

Eq. (15) becomes identical to Eq. (14) if the first term on the RHS is dropped, as Helliwell does in his next equation. The "quasi-longitudinal approximation" of classical linear whistler theory is in fact equivalent to dropping the component of displacement current parallel[1] to $\mathbf{k}$, while the neglect of the first term in (15) is equivalent to dropping the component of displacement current transverse to $\mathbf{k}$. Our model does both, in the context of the full *nonlinear* Maxwell/fluid equations. Helliwell shows that the quasi-longitudinal approximation is accurate as long as

$$\frac{\sin^2\theta}{\cos\theta} < \frac{2\omega_{pc}^2}{3\omega\Omega} \tag{16}$$

for typical parameters of interest, this range extends from $\theta = 0$ nearly to $\theta = 90°$. It is of interest to compare this range of validity with the range of propagation angles for whistlers. According to Eq. (14) (and the exact

[1] In conventional plasma parlance the component parallel to $\mathbf{k}$ is called the longitudinal displacement current, but in the older literature the word "longitudinal" is also used with the very different meaning "parallel to $\mathbf{B}$". The term "quasi-longitudinal approximation" refers to this latter meaning. To confuse matters even further, it turns out (Eq. (16)) that the "quasi-longitudinal approximation" is valid for θ up to nearly 90°.

Maxwell equations lead to exactly the same condition [1]), propagating whistlers (i.e., waves with real k) occur only if

$$\cos\theta > \frac{\omega}{\Omega}. \tag{17}$$

Except for whistlers with ω nearly exactly equal to Ω, Helliwell's validity condition (16) is well satisfied over the entire range of angles θ that permit propagating waves. Thus, the approximations made in our model appear to be very well justified as long as $\omega \ll \omega_{pc}$ and $\omega < 0.9\Omega$.

4. Finite-difference solution procedure: numerical stability

As a test of the numerical accuracy and stability of finite-difference schemes to solve Eqs. (6), (9), (2), and (3), we consider the case of a single linear mode with spatial dependence e^{ikz}. In the present section, we choose coordinates so that **B** is along the z-axis, and to simplify the algebra we assume **k** is parallel to **B**, but the result is the same for oblique modes. For this case of parallel propagation, Eqs. (10) and (11) can be reduced to the single equation

$$\frac{\partial \mathbf{v}_c}{\partial t} = -\omega_0 \hat{\mathbf{i}}_z \times \mathbf{v}_c, \tag{18}$$

where $\hat{\mathbf{i}}_z$ is the unit vector along the magnetic field and

$$\omega_0 \equiv \frac{k^2c^2}{\omega_{pc}^2 + k^2c^2}\Omega \tag{19}$$

is the wave frequency from Eq. (14). Using the complex spinor notation $u \equiv v_x + iv_y$, Eq. (18) becomes simply

$$\frac{\partial u}{\partial t} = -i\omega_0 u. \tag{20}$$

Thus, it is clear that the essential operation in our algorithm is simply a rotation, and the exact solution to (20) is

$$u = u_0 e^{-i\omega t}, \tag{21}$$

neutrally stable, with real ω equal to ω_0.

The linearized single-mode equation (20) could be solved with an implicit finite-difference scheme; in fact, there are tricks that can be used to perform rotations exactly when one has prior knowledge of the angle of rotation per time step [7,8]. However, our complete model equations (6) and (9) can only be solved explicitly, by using (9) to solve for **E** and $\mathbf{v}_c$ at a given time step, and then using this value of **E** in (6) to push $\mathbf{v}_c$ to the next time step. Since this procedure is not time-centered, it is necessary (for both accuracy and stability) to iterate the finite time step to perform the rotation as accurately as possible. We can use (20) as a simple model to guide us in the specification of a stable and accurate finite-difference procedure. For any given finite-difference procedure, the solution to (20) will be of the form (21), but ω will not be equal to the exact result ω_0. Errors in the real part of ω represent phase inaccuracy, while errors in the imaginary part represent unphysical instability or damping; these latter types of errors are particularly serious since they exponentiate over time.

The explicit finite-difference form of (20) is

$$\frac{u_1 - u_0}{\tau} = -i\omega_0 u_0, \tag{22}$$

where τ is the time step, u_0 is the value at the beginning of the time step, and u_1 is this first approximation to the value at the end of the time step. Setting $u_1 = u_0 e^{-i\omega_1\tau}$, the solution to (22) is

$$\omega_1 = \frac{i}{\tau}\ell n(1 - i\omega_0\tau) \approx \omega_0 + \frac{1}{2}i\omega_0^2\tau - \frac{1}{3}\omega_0^3\tau^2, \tag{23}$$

where we have expanded in the small parameter $\omega_0\tau$. The solution is unstable to first order in τ, which is unacceptable.

To improve the time-centering, we can use a predictor–corrector iteration, i.e., we define an improved approximation to Eq. (20) by

$$\frac{u_2 - u_0}{\tau} = -\mathrm{i}\omega_0 \frac{u_0 + u_1}{2}. \tag{24}$$

Setting $u_2 = u_0 \mathrm{e}^{-\mathrm{i}\omega_2 \tau}$, the solution to (24) is

$$\omega_2 = \frac{\mathrm{i}}{\tau} \ell n \left(1 - \mathrm{i}\omega_0 \tau - \frac{1}{2}\omega_0^2 \tau^2\right) \approx \omega_0 + \frac{1}{6}\omega_0^3 \tau^2 + \frac{1}{8}\mathrm{i}\omega_0^4 \tau^3. \tag{25}$$

The solution is still unstable, but the growth rate is now third-order in $\omega_0\tau$, and the real part of ω is accurate to second order. In some cases, this is quite adequate. If τ is chosen to be $1/8\Omega$, the code can be run $2^{15} = 32{,}768$ time steps before the numerical instability causes the whistler with $\omega \approx \Omega$ to amplify by one e-fold.

However, it is possible to further improve the accuracy and stability by several orders of magnitude at minimal additional cost. To do this, we first perform a second corrector step, defining

$$\frac{u_3 - u_0}{\tau} = -\mathrm{i}\omega_0 \frac{u_0 + u_2}{2}. \tag{26}$$

The solution to (26) is

$$\omega_3 = \frac{\mathrm{i}}{\tau} \ell n \left(1 - \mathrm{i}\omega_0 \tau - \frac{1}{2}\omega_0^2 \tau^2 + \frac{1}{4}\mathrm{i}\omega_0^3 \tau^3\right) \approx \omega_0 + \frac{1}{12}\omega_0^3 \tau^2 - \frac{1}{8}\mathrm{i}\omega_0^4 \tau^3 + \frac{3}{40}\omega_0^5 \tau^4 - \frac{1}{32}\mathrm{i}\omega_0^6 \tau^5. \tag{27}$$

This solution is damped in third order; the correction has overshot and turned instability into damping, at exactly the same rate. This may be regarded as an improvement, since numerical damping is preferable to numerical instability, but we can obtain a really impressive advance in numerical stability by setting our solution u to the *average* of u_2 and u_3. We then find

$$\omega = \frac{\mathrm{i}}{\tau} \ell n \left(1 - \mathrm{i}\omega_0 \tau - \frac{1}{2}\omega_0^2 \tau^2 + \frac{1}{8}\mathrm{i}\omega_0^3 \tau^3\right) \approx \omega_0 + \frac{1}{24}\omega_0^3 \tau^2 + \frac{1}{80}\omega_0^5 \tau^4 + \frac{1}{128}\mathrm{i}\omega_0^6 \tau^5. \tag{28}$$

This solution is unstable, but only to fifth order in $\omega_0\tau$, and even in the fifth-order error the coefficient is extremely small. Using a time step $\tau = 1/4\Omega$, the code can be run $2^{19} = 524{,}288$ time steps before any whistler grows by one e-fold due to the numerical error. If the time step is $1/10\Omega$, the code can be run 10^8 time steps before any whistler grows by one e-fold. For practical purposes, this amounts to perfect stability. Thus, this is the procedure that we follow in our numerical solution. Specifically, our solution procedure is as follows:

1. Start with $\mathbf{v}_n$, $\mathbf{E}_n$, $\mathbf{B}_n$, the known values of $\mathbf{v}$, $\mathbf{E}$, $\mathbf{B}$ at time step n.
2. Use $\mathbf{E}_n$ in (6) to push $\mathbf{v}$ to time step $n+1$. Call the result $\mathbf{v}^{(1)}_{n+1}$, the first iteration to $\mathbf{v}_{n+1}$.
3. Solve Eqs. (2) and (3) for $\mathbf{B}^{(1)}_{n+1}$, using $\mathbf{v}^{(1)}_{n+1}$ on the RHS.
   Solve Eq. (9) for $\mathbf{E}^{(1)}_{n+1}$, using $\mathbf{v}^{(1)}_{n+1}$ and $\mathbf{B}^{(1)}_{n+1}$ on the RHS.
4. Repeat step (2), now using $\mathbf{E}^{(1)}_{n+1/2} \equiv (\mathbf{E}_n + \mathbf{E}^{(1)}_{n+1})/2$ on the RHS. Call the result $\mathbf{v}^{(2)}_{n+1}$.
5. Repeat step (3), using $\mathbf{v}^{(2)}_{n+1}$ and $\mathbf{B}^{(2)}_{n+1}$ on the RHS.
6. Repeat step (2) one more time, using $\mathbf{E}^{(2)}_{n+1/2} \equiv (\mathbf{E}_n + \mathbf{E}^{(2)}_{n+1})/2$ on the RHS. Call the result $\mathbf{v}^{(3)}_{n+1}$.
7. Repeat step (3) again, using $\mathbf{v}^{(3)}_{n+1}$ and $\mathbf{B}^{(3)}_{n+1}$ on the RHS.
8. Set $\mathbf{v}_{n+1} \equiv (\mathbf{v}^{(2)}_{n+1} + \mathbf{v}^{(3)}_{n+1})/2$, $\mathbf{E}_{n+1} \equiv (\mathbf{E}^{(2)}_{n+1} + \mathbf{E}^{(3)}_{n+1})/2$, and $\mathbf{B}_{n+1} \equiv (\mathbf{B}^{(2)}_{n+1} + \mathbf{B}^{(3)}_{n+1})/2$.
9. Proceed to the next time step.

Actual code runs are found to agree with Eq. (28) nearly exactly. As an example, Fig. 1(a) shows the time dependence of the wave amplitude for a whistler initiated in cold plasma with frequency $\omega = 0.69\Omega$. In this run the time step is $\tau = 1/4\Omega$, the system length is 64 grid points, and the initiated wave is mode three, i.e., 21.33 grid points per wavelength. In an exact solution, the whistler would be neutrally stable. After 20,000 time steps, Eq. (28) predicts wave growth by a factor 1.0041, which (to five-figure accuracy) is exactly what is found. For purposes of comparison, Fig. 1(b) shows the same wave simulated using a simple double-corrector

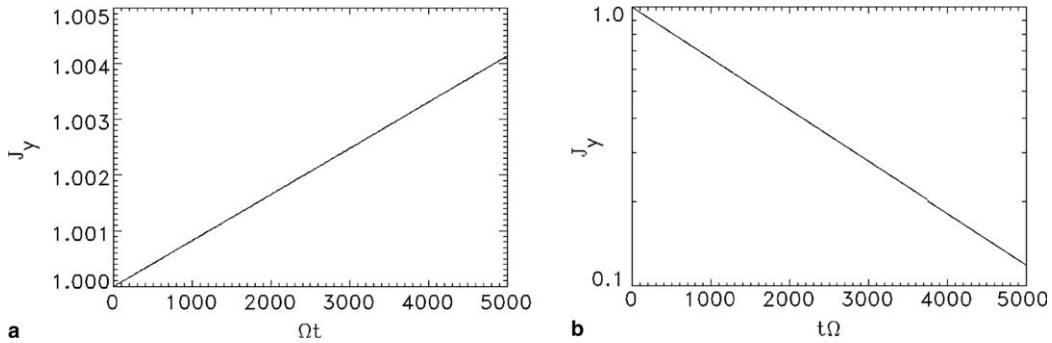

Fig. 1. (a) HEMPIC simulation showing the amplitude J_y of a stable whistler launched in cold plasma. Over 20,000 time steps, the amplitude grows by a factor 1.004 due to numerical instability, in exact agreement with Eq. (28). (b) The same simulation using a simple double-corrector algorithm. In this case, the wave decays by a factor 0.11, in good agreement with Eq. (27).

scheme, without averaging the first and second corrections, i.e., stopping at step (7) above. The predicted result from Eq. (27) is then exponential wave damping by a factor 0.11; the actual result shown in Fig. 1(b) is exponential decay by a factor 0.12.

5. Inclusion of PIC simulation particles in addition to the cold fluid

We now consider the electron distribution to consist of a set of simulation particles, in addition to the cold fluid component that has been considered previously. In typical applications, the simulation particles may represent the energetic portion of the electron distribution, or the class of electrons that are cyclotron resonant with the waves and therefore exhibit nonlinear behaviors that can only be represented at the kinetic level. Treating these simulation particles fully relativistically, the equations of motion for the jth particle are:

$$\frac{\mathrm{d}\mathbf{p}_j}{\mathrm{d}t} = -e\mathbf{E} - \frac{e\mathbf{v}_j \times \mathbf{B}}{c}, \tag{29}$$

$$\frac{\mathrm{d}\mathbf{x}_j}{\mathrm{d}t} = \mathbf{v}_j, \tag{30}$$

where $\mathbf{p}_j \equiv m\gamma_j\mathbf{v}_j$ is the momentum and $\gamma_j \equiv (1 + p_j^2/m^2c^2)^{-1/2}$ is the relativistic mass factor. In the usual fashion for a PIC code, the fields are interpolated to the particle position from a grid, and conversely the particles are laid down onto the grid to specify the particle density n_p and the particle current $\mathbf{J}_\mathrm{p}$ at each grid point. We shall see below that it is also necessary to lay down several other moments of the particle velocity distribution in the same way. Now the equations that determine the fields $\mathbf{E}$ and $\mathbf{B}$, and the cold-fluid density n_c and velocity $\mathbf{v}_\mathrm{c}$, are the generalizations of Eqs. (2), (3), (5), (6), and (9) to include n_p and $\mathbf{J}_\mathrm{p}$. The quasineutrality condition becomes

$$n_\mathrm{c}(\mathbf{x}, t) + n_\mathrm{p}(\mathbf{x}, t) = n_0(\mathbf{x}), \tag{31}$$

where now both n_c and n_p can vary with time, but their sum must be time-independent. (However, $n_\mathrm{p}/n_\mathrm{c}$ is often so small that n_c can be regarded as time-independent for all practical purposes.) By analogy with Eq. (6), the equation

$$\frac{\partial \mathbf{J}_\mathrm{c}}{\partial t} = -\frac{c^2}{4\pi}\nabla \times \nabla \times \mathbf{E} - \frac{\partial \mathbf{J}_\mathrm{p}}{\partial t} \tag{32}$$

is used to push the cold-fluid current $\mathbf{J}_\mathrm{c} \equiv -n_\mathrm{c}e\mathbf{v}_\mathrm{c}$, and the fields are determined by

$$\nabla \times \mathbf{B} = \frac{4\pi}{c}(\mathbf{J}_\mathrm{c} + \mathbf{J}_\mathrm{p}) \tag{33}$$

and

$$\nabla \times \nabla \times \mathbf{E} + \frac{\omega_\mathrm{pc}^2}{c^2}\mathbf{E} = \frac{4\pi}{c^2}\nabla \cdot (\mathbf{v}_\mathrm{c}\mathbf{J}_\mathrm{c}) - \frac{\omega_\mathrm{pc}^2}{c^3}\mathbf{v}_\mathrm{c} \times \mathbf{B} - \frac{4\pi}{c^2}\frac{\partial \mathbf{J}_\mathrm{p}}{\partial t}, \tag{34}$$

where $\omega_\mathrm{pc} \equiv (4\pi n_\mathrm{c}e^2/m)^{1/2}$.

In a finite-difference implementation, Eqs. (31)–(34) are used at each time step to determine the quantities on the LHS, and the quantities on the RHS are regarded as known. Just as in the case of the cold fluid, the time derivatives of $\mathbf{J}_\mathrm{p}$ on the RHS of Eqs. (32) and (34) lead to numerical problems. To eliminate these time derivatives, we use the momentum equation for the particles, treated as a relativistic warm fluid, which can be derived by taking the velocity moment of the relativistic Vlasov equation. In analytic form, this equation is

$$\frac{\partial \mathbf{J}_\mathrm{p}}{\partial t} = e\nabla\cdot\int \mathrm{d}^3\mathbf{v}\mathbf{v}\mathbf{v} f_\mathrm{p}(\mathbf{x},\mathbf{v},t) + \frac{e^2}{m}\mathbf{E}\cdot\int \mathrm{d}^3\mathbf{v}\frac{f_\mathrm{p}(\mathbf{x},\mathbf{v},t)}{\gamma(v)}\left(\mathbf{I}-\frac{\mathbf{v}\mathbf{v}}{c^2}\right) - \frac{e^2}{mc}\mathbf{B}\times\int \mathrm{d}^3\mathbf{v}\mathbf{v}\frac{f_\mathrm{p}(\mathbf{x},\mathbf{v},t)}{\gamma(v)}, \tag{35}$$

where $f_\mathrm{p}(\mathbf{x},\mathbf{v},t)$ is the distribution function of the simulation particles, and $\mathbf{I}$ is the unit dyadic tensor. In the PIC code, each of the integrals is evaluated on the grid by laying down the relevant simulation particle quantity.

If the simulation particles are non-relativistic, γ is unity for all particles and then Eqs. (32), (34) and (35) may be written in the more compact form:

$$\frac{\partial \mathbf{J}_\mathrm{c}}{\partial t} = -\frac{c^2}{4\pi}\nabla\times\nabla\times\mathbf{E} - \frac{e}{m}\nabla\cdot\mathbf{K}_\mathrm{p} - \frac{\omega_\mathrm{pp}^2}{4\pi}\mathbf{E} - \frac{e\mathbf{B}\times\mathbf{J}_\mathrm{p}}{mc}, \tag{36}$$

$$\nabla\times\nabla\times\mathbf{E} + \frac{\omega_\mathrm{p}^2}{c^2}\mathbf{E} = -\frac{4\pi}{c^2}\nabla\cdot(\mathbf{v}_\mathrm{c}\mathbf{J}_\mathrm{c}) - \frac{4\pi e\mathbf{B}\times(\mathbf{J}_\mathrm{c}+\mathbf{J}_\mathrm{p})}{mc} - \frac{4\pi e}{m}\nabla\cdot\mathbf{K}_\mathrm{p}, \tag{37}$$

where $\omega_\mathrm{pp} = (4\pi n_\mathrm{p} e^2/m)^{1/2}$ is the non-relativistic simulation particle plasma frequency, $\omega_\mathrm{p} = [4\pi(n_\mathrm{c}+n_\mathrm{p})e^2/m]^{1/2}$ is the total plasma frequency, and $\mathbf{K}_\mathrm{p}(x,t) \equiv \int \mathrm{d}^3\mathbf{v}\mathbf{v}\mathbf{v} f_\mathrm{p}(\mathbf{x},\mathbf{v},t)$ is the simulation particle stress tensor.

Note that the particles are advanced using Newton's equations of motion (29) and (30), but the cold-fluid velocity $\mathbf{v}_\mathrm{c}$, or equivalently the fluid current $\mathbf{J}_\mathrm{c}$, is advanced by using Eq. (36), which ultimately derives from the quasi-neutrality requirement. Our quasineutral scheme could not be implemented in a pure PIC code, without the presence of the cold-fluid electrons.

To advance equations (29)–(35) from time step n to time step $n+1$, we can use essentially the same predictor–corrector–corrector scheme that was prescribed at the end of Section 4. We first outline a numerical procedure that is applicable quite generally. In the following paragraph, we give a short-cut that can be used when $n_\mathrm{p}/n_\mathrm{c} \ll 1$. The general procedure is:

1. Start with $\mathbf{E}_n$, $\mathbf{B}_n$, n_{cn}, $\mathbf{J}_{cn}$, $\{\mathbf{x}_{jn},\mathbf{p}_{jn}\}$, the known values of the fields, cold-fluid density n_c and current $\mathbf{J}_\mathrm{c}$, and particle positions/momenta at time step n.
2. Use $\mathbf{E}_n$ and $\mathbf{B}_n$ in (29) and (30) to push $\{\mathbf{x}_j,\mathbf{p}_j\}$ to time step $n+1$, and call the result $\{\mathbf{x}^{(1)}_{j,n+1},\mathbf{p}^{(1)}_{j,n+1}\}$. Take care that the particle push resolves wavelength scales.
3. Lay down the particle phase space coordinates $\{\mathbf{x}^{(1)}_{j,n+1},\mathbf{v}^{(1)}_{j,n+1}\}$ on the grid to form up $n^{(1)}_{p,n+1}$, $\mathbf{J}^{(1)}_{p,n+1}$, and the various moments that appear in Eq. (35). Define $n^{(1)}_{p,n+1/2} \equiv (n_{pn}+n^{(1)}_{p,n+1})/2$, and similarly for $\mathbf{J}^{(1)}_{p,n+1/2}$ and the other moments.
4. Use $\mathbf{E}_n$, $\mathbf{B}_n$, $n^{(1)}_{p,n+1/2}$, $\mathbf{J}^{(1)}_{p,n+1/2}$, and the other moments at time $n+1/2$ in (32) to push $\mathbf{J}_\mathbf{c}$ to time step $n+1$. Call this value $\mathbf{J}^{(1)}_{c,n+1}$.
5. Solve Eqs. (34) and (35) for $\mathbf{E}^{(1)}_{n+1}$, using $\mathbf{J}^{(1)}_{c,n+1}$, $\mathbf{J}^{(1)}_{p,n+1}$, and the various moments at time $n+1$ on the RHS. Solve Eqs. (33) and (3) for $\mathbf{B}^{(1)}_{n+1}$, using $\mathbf{J}^{(1)}_{c,n+1}$, $\mathbf{J}^{(1)}_{p,n+1}$ on the RHS.
6. Repeat steps (2–5), using $\mathbf{E}^{(1)}_{n+1/2} \equiv (\mathbf{E}_n+\mathbf{E}^{(1)}_{n+1})/2$ and $\mathbf{B}^{(1)}_{n+1/2} \equiv (\mathbf{B}_n+\mathbf{B}^{(1)}_{n+1})/2$ on the RHS.
7. Repeat steps (2–5) again, using $\mathbf{E}^{(2)}_{n+1/2} \equiv (\mathbf{E}_n+\mathbf{E}^{(2)}_{n+1})/2$ and $\mathbf{B}^{(2)}_{n+1/2} \equiv (\mathbf{B}_n+\mathbf{B}^{(2)}_{n+1})/2$ on the RHS.
8. Set $\mathbf{x}_{j,n+1} \equiv (\mathbf{x}^{(2)}_{j,n+1}+\mathbf{x}^{(3)}_{j,n+1})/2$, and similarly for $\mathbf{p}_{j,n+1}$, $\mathbf{J}_{c,n+1}$, $\mathbf{E}_{n+1}$, and $\mathbf{B}_{n+1}$.
9. Proceed to the next time step.

In many problems of interest, the population of resonant electrons is small and $n_\mathrm{p}/n_\mathrm{c} \ll 1$. In this case, the PIC particles only slowly influence the evolution of the wave. It is then quite adequate to first advance the

wave from time step n to time step $n+1$, using the procedure of Section 4, which involves only the cold fluid, and then afterwards to use leapfrog to advance the particles. This avoids the need to push the particles three times at each time step.

6. Energy conservation

Since our model is based on an approximation to Maxwell's equation, it is important to determine whether the model conserves energy. We now address this issue.

Let $\epsilon_{\rm kin}$ be the total kinetic energy density of the plasma (including the kinetic energy of the cold-fluid electrons, as well as the ordered and thermal kinetic energy of the particle electrons). Since our model includes the exact equations of motion for the particle electrons, as well as the exact momentum equation for the cold-fluid electrons,

$$\frac{\partial \varepsilon_{\rm kin}}{\partial t} = \mathbf{J}\cdot\mathbf{E} + \nabla\cdot\mathbf{Q}, \tag{38}$$

where $\mathbf{J}\cdot\mathbf{E}$ is the work done on the plasma, per unit volume, and $\mathbf{Q}$ is the standard heat flux plus convective energy flow. Using Eq. (33) to substitute for $\mathbf{J}$ and using a vector identity, we find

$$\mathbf{J}\cdot\mathbf{E} = \frac{c}{4\pi}\mathbf{E}\cdot(\nabla\times\mathbf{B}) \equiv \frac{c}{4\pi}[\mathbf{B}\cdot(\nabla\times\mathbf{E}) - \nabla\cdot(\mathbf{E}\times\mathbf{B})]. \tag{39}$$

Now using Eq. (1) to eliminate $\nabla\times\mathbf{E}$, we find

$$\mathbf{J}\cdot\mathbf{E} = -\nabla\cdot\frac{c}{4\pi}(\mathbf{E}\times\mathbf{B}) - \frac{\partial}{\partial t}\frac{\mathbf{B}^2}{8\pi}. \tag{40}$$

Thus, we can write Eq. (38) in the conservative form

$$\frac{\partial \varepsilon}{\partial t} = \nabla\cdot(\mathbf{Q}+\mathbf{S}), \tag{41a}$$

where

$$\mathbf{S} \equiv c(\mathbf{E}\times\mathbf{B})/4\pi \tag{41b}$$

and

$$\varepsilon \equiv \varepsilon_{\rm kin} + \frac{B^2}{8\pi}. \tag{41c}$$

Note that the Poynting electromagnetic energy flux S is exact, but the electric field energy $E^2/8\pi$ is omitted from ε; this is due to our neglect of the displacement current. Since $|E| = (\omega/kc)|B|$, this is consistent with our basic assumption that $|\omega/kc| \ll 1$. Thus, the equations of our model satisfy an energy conservation law, albeit with a slightly modified definition of field energy.

Of course, this does not necessarily mean that there will be exact conservation in a finite-difference fluid/PIC implementation. In cases where HEMPIC is run with the plasma represented entirely as a cold fluid, we find that the energy grows systematically and extremely slowly in exact agreement with the numerical stability calculation presented in Section 4. For example, for the case shown in Fig. 1, the wave amplitude grows by a factor 1.004 over 20,000 time steps, and the total energy grows systematically by a factor 1.008, i.e., as the square of the amplitude. In cases where the plasma is represented as a cold fluid plus simulation particles, we find that energy fluctuates a bit, due to the statistical noise associated with the finite number of particles. These fluctuations easily dominate over any systematic effects, but they are well within the normal expectations for a PIC code, e.g. on the order of $\pm 0.5\%$ in the case shown in the following section, where an unstable whistler grows by three orders of magnitude over a time $600/\Omega$, comprising 2400 time steps $\tau = 1/4\Omega$.

7. Example: Growth and saturation of whistler instability

Our primary motivation for developing the HEMPIC code is to study the nonlinear physics of whistler instability, amplification, and triggering in the magnetosphere. There is an enormous database in this area (see, e.g. the review by Helliwell [9]), and considerable effort has been devoted to theoretical and numerical studies (see, e.g. [6,10–13]), but computational efficiency has been a limiting factor. It is thought that finite wavepacket length, and spatial variation of both the plasma density and the ambient field, play an essential role in the nonlinear evolution of resonant electron/whistler interactions [6,10,11]. However, we shall defer HEMPIC studies that include these effects to future publications. In the present paper, we consider a convenient nonlinear test problem that is amenable to analytic solution: the whistler instability that occurs in homogeneous plasma with an electron distribution of the form

$$f(\mathbf{p}) = n_c\delta(\mathbf{p}) + \frac{n_p}{2\pi p_{\perp 0}}\delta(p_\perp - p_{\perp 0})\delta(p_z - p_{z0}), \tag{42}$$

i.e., a cold plasma component plus a ring distribution of energetic electrons. We shall assume that $n_p \ll n_c$. In Eq. (42) the momentum $\mathbf{p}$ is written in cylindrical coordinates, with the magnetic field taken to be along the z-axis.

To set the simulations in context, we begin with a brief presentation of the linear and nonlinear theory for unstable whistlers in this situation. Considering only modes propagating along z, and beginning with the exact expression for the electron susceptibility (Eq. (10.48) of [1]), one can derive the exact linear dispersion relation

$$0 = \frac{k^2c^2}{\omega^2} - \frac{\omega_{pc}^2}{\Omega - \omega} + \frac{\omega_{pp}^2}{\omega\gamma_0}\frac{\omega - kv_{z0}}{\omega - kv_{z0} - \Omega/\gamma_0} - \frac{\omega_{pp}^2}{2\omega\gamma_0}\frac{v_{\perp 0}^2}{c^2}\frac{\omega^2 - k^2c^2}{(\omega - kv_{z0} - \Omega/\gamma_0)^2}, \tag{43}$$

where $v_{z0} \equiv p_{z0}/m\gamma_0$, $v_{\perp 0} \equiv p_{\perp 0}/m\gamma_0$, $p_0^2 \equiv p_{z0}^2 + p_{\perp 0}^2$, and $\gamma_0 \equiv (1 + p_0^2/m^2c^2)^{1/2}$. Instability occurs for modes that are in cyclotron resonance with the fast electrons, i.e., values of k that satisfy

$$\omega(k) - kv_{z0} - \Omega/\gamma_0 = 0. \tag{44}$$

The instability is due to the second-order pole in the last term of (43), and it is driven by the transverse energy of the ring distribution. (Note that the coefficient of this term is proportional to $v_{\perp 0}^2$. The preceding first-order pole term has no dependence on $v_{\perp 0}^2$, and it does not lead to instability.) To obtain an analytic solution to the dispersion relation, we treat the resonant electrons (last two terms of (43)) as a perturbation, and write the frequency $\omega(k)$ as

$$\omega(k) \equiv \omega_0(k) + \delta\omega(k), \tag{45}$$

where $\omega_0(k)$, given by Eq. (19), is the unperturbed frequency due to only the cold electrons. We let k_0 be the solution of the resonance condition (44) with $\omega(k)$ given by $\omega_0(k)$. Using (45) to expand (43), and keeping only lowest orders in $\delta\omega$, we find

$$[\delta\omega(k_0)]^3 = \frac{v_{\perp 0}^2}{2c^2}\frac{\omega_{pp}^2(k_0^2c^2 - \omega_{00}^2)}{\gamma_0\omega_{00}}\left(\frac{k_0^2c^2}{\omega_{00}^2} + \frac{\omega_{pc}^2}{(\Omega - \omega_{00})^2}\right)^{-1}, \tag{46}$$

where $\omega_{00} \equiv \omega_0(k_0)$. There is one unstable root, with a growth rate of order $(n_p/n_c)^{1/3}$, and a frequency shift $\mathrm{Re}(\delta\omega)$ which is of the same order and negative, since $k_0^2c^2 > \omega_0^2$ for a whistler. The instability thus formally resembles a cold-beam two-stream instability. (There would still be an instability if $k_0^2c^2$ were less than ω_0^2, but in that case it would formally resemble the negative-mass instability that is associated with the azimuthal bunching in gyrotrons [14].)

The nonlinear theory of the single-mode instability begins with the equation of motion (29) of the particles. Assuming that the wave electric field is of the form $\mathbf{E}(t)\exp\left(\mathrm{ikz} - i\int_0^t \omega(t')\,\mathrm{d}t'\right)$, where $E(t)$ and $\omega(t)$ are slowly varying (compared to the time scale ω), the vector equation (29) can be reduced to three scalar equations:

$$\frac{\partial p_\perp}{\partial t} = -eE\left(1 - \frac{kv_z}{\omega}\right)\cos\psi, \tag{47a}$$

$$\frac{\partial p_z}{\partial t} = -eE\frac{kv_\perp}{\omega}\cos\psi, \tag{47b}$$

$$\frac{\partial \psi}{\partial t} = -\frac{eE}{p_\perp}\left(1 - \frac{kv_z}{\omega}\right)\sin\psi + kv_z - \omega + \Omega/\gamma, \tag{47c}$$

where $\varphi \equiv \tan^{-1}(p_y/p_x)$ is the phase of the electron momentum $\mathbf{p}_\perp$, and $\psi \equiv \varphi - kz + \int_0^t \omega(t')\,dt'$ is the phase difference between the electron and the wave. Note that the fast timescale has been removed from these equations; $p_\perp$, p_z, and ψ are all variables that vary slowly compared to the gyrofrequency Ω or the wave frequency ω.

The equations can be further simplified by expanding in the small parameter ω/kv_z, the ratio of the wave electric field to the wave magnetic field. To lowest order in this parameter, Eq. (47) indicates that $p^2 \equiv p_\perp^2 + p_z^2$ is constant. (Kinetic energy is conserved because the forces on the electron are, to this order of approximation, magnetic.) Thus, it is preferable to express $\mathbf{p}$ in rotating spherical coordinates (p,α,ψ), where $\alpha \equiv \tan^{-1}(p_\perp/p_z)$ is the pitch angle. Eq. (47) then becomes

$$\frac{d\alpha}{dt} = \frac{keE}{m\gamma\omega}\cos\psi, \tag{48a}$$

$$\frac{d\psi}{dt} = -\frac{keE}{m\gamma\omega}\cot\alpha\sin\psi + kv\cos\alpha - \omega + \frac{\Omega}{\gamma}. \tag{48b}$$

The coupled nonlinear equations (48a) and (48b) for α and ψ have a fixed point (α_0,ψ_0), where $\psi_0 = \pi/2$ (i.e., particle velocity in phase with the wave magnetic field), and α_0 is the solution of a nonlinearly modified resonance condition

$$\frac{keE}{m\gamma\omega}\cot\alpha_0\sin\psi = kv\cos\alpha_0 - \omega + \frac{\Omega}{\gamma}. \tag{49}$$

The value of ψ for non-resonant electrons rapidly cycles through the full range 0–2π, but when E becomes large enough, electrons whose pitch angle α and relative phase ψ lie close to (α_0,ψ_0) become trapped in phase, and (α,ψ) perform small oscillations about (α_0,ψ_0). This phenomenon of phase trapping is analogous [15] to the longitudinal velocity trapping that occurs in the electrostatic two-stream instability [16], and as in that case the trapped electrons exchange energy back and forth with the wave over the course of a trapping oscillation. As a result, the linear instability saturates when trapping sets in, and the wave amplitude subsequently oscillates at the trapping frequency [16].

Figs. 2–5 show some results of a one-dimensional HEMPIC simulation, with $\omega_{pc}/\Omega = 8$, $n_p/n_c = 10^{-4}$, $v_{z0}/c = 1/5$, and $v_{\perp 0}/c = 1/5$. For these parameters, the unstable wave has $\omega_0 = \Omega/5$. The simulation uses 64 grid cells per wavelength, 20,000 particles, and the time step is $\tau = 1/4\Omega$. Simulation particles are used

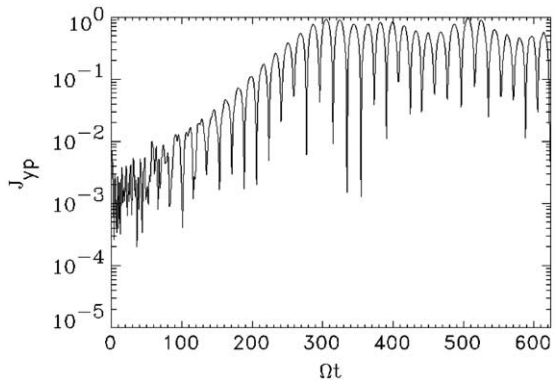

Fig. 2. Time evolution of J_{yp}, plotted on a semi-log scale, for a whistler driven unstable by a ring distribution of energetic electrons.

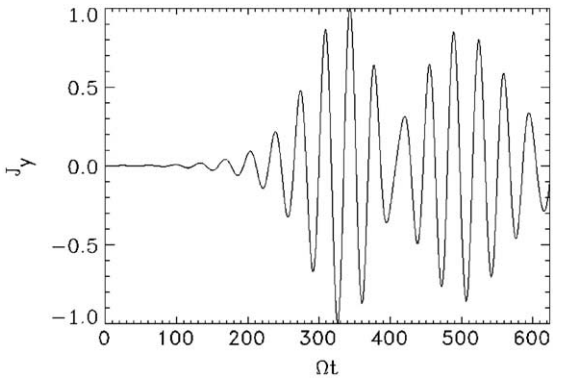

Fig. 3. Time evolution of J_{yc}, plotted on a linear scale, from the simulation of Fig. 2.

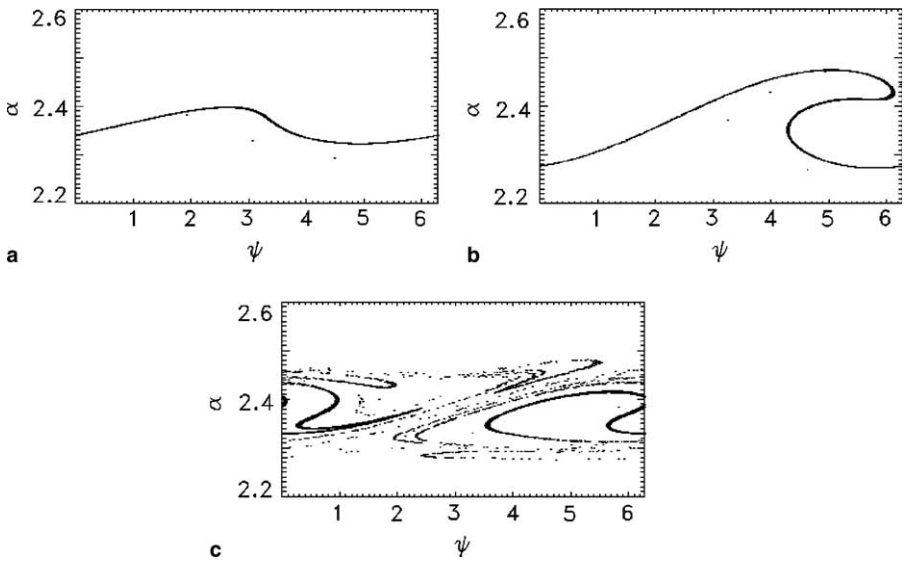

Fig. 4. Snapshots of the particle distribution in the phase space (ψ vs. α), (a) late in the linear growth phase, at $t = 270/\Omega$; (b) during the onset of electron phase trapping, at $t = 330/\Omega$; (c) after several trapped-particle oscillations, at $t = 600/\Omega$.

to represent the ring distribution of energetic electrons in Eq. (42). In Fig. 2, we show the temporal growth of the simulation-particle current component J_{yp} on a semi-log scale. The instability is seen to grow exponentially over three orders of magnitude, with a growth rate 0.024Ω, in excellent agreement with the predicted exponential growth rate 0.026Ω from Eq. (46). Over the course of the run, the total energy ϵ defined in Eq. (41c) is conserved to within $\pm 0.5\%$. Fluctuations in energy seem to be due primarily to the noise associated with the finite number of particles, rather than the finite time step or any systematic tendency in the algorithm. Fig. 3 shows the cold-electron current component J_{yc} on a linear scale. This figure shows clearly the saturation and subsequent oscillation of the wave amplitude. Fig. 4 shows snapshots of the simulation particles in the 2-D cross-section of phase space (ψ vs. α), at three different times. This figure shows the phase trapping of the resonant electrons, which becomes quite complex at late times due to anharmonic effects and to the slow oscillation of the wave amplitude. Fig. 5 shows the simulation particle distribution in the phase space cross-section (p_y vs. z), showing how the particles become phase-bunched as the wave grows, and then how the bunching spreads out after the particles are trapped. This is a phenomenon that was emphasized by Helliwell and Crystal [17] early in the study of whistler instabilities.

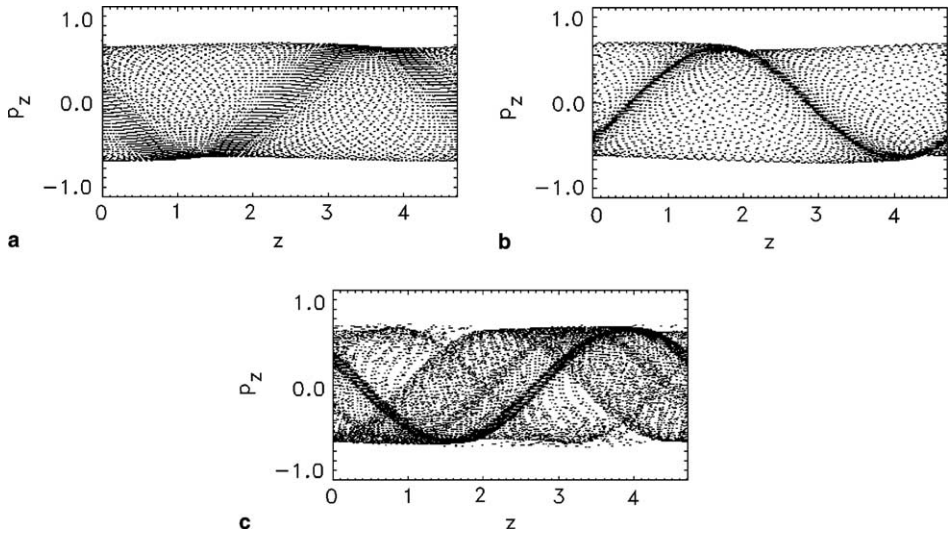

Fig. 5. Snapshots of the electron distribution in the phase space (p_y vs. z), showing (a) the onset of phase bunching late in the linear growth phase, at $t = 270/\Omega$; (b) nearly complete bunching shortly after saturation, at $t = 330/\Omega$, and (c) spreading of the bunches after several trapped-particle oscillations have occurred, at $t = 600/\Omega$.

8. Example: Ducting of whistler in narrow channels

It is known that whistlers can be guided along the magnetic field by both field-aligned plasma density enhancements and plasma density depletions [2,18]. Traditionally, ray tracing and WKB analysis have been used to study the physics underlying these ducting processes. However, there are experiments in the literature [19–21] showing ducting in very narrow channels, comparable to the whistler wavelength, and the details of these experiments have never been explained. In narrow density channels, it is necessary to use a full-wave analysis. We are in the process of completing such an analysis, which will be the subject of a future publication.

HEMPIC has proven quite useful in simulating ducting over a wide range of conditions, and we shall show an example in Fig. 6. In these simulations, the plasma is represented entirely as a cold fluid, so that the

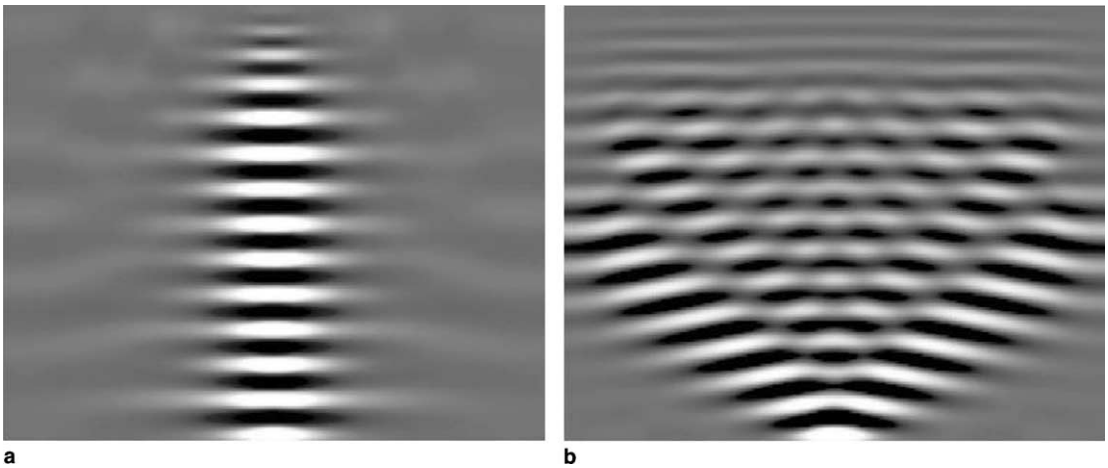

Fig. 6. (a) HEMPIC simulation of a ducted whistler in an enhanced-density channel. (b) The same whistler launched into uniform plasma. In these figures, the horizontal scale runs from $-1.82c/\Omega$ to $+1.82c/\Omega$, while the vertical scale runs from zero to $15.5c/\Omega$.

whistlers are stable, and the waves that are launched are in the linear regime. A whistler with frequency $\omega = \Omega/10$ is launched at $(x = 0, z = 0)$, within an enhanced-density channel with profile

$$n(x) = n_{\text{out}} + \frac{1}{2}(n_{\text{out}} - n_{\text{in}})\left[\tanh\left(\frac{x - x_d}{x_g}\right) - \tanh\left(\frac{x + x_d}{x_g}\right)\right]. \tag{50}$$

Here, the channel half-width is $x_d = 0.18\ c/\Omega$, the channel edge sharpness is $x_g = 0.036c/\Omega$, the density ratio is $n_{\text{in}}/n_{\text{out}} = 4$, and $\omega_{\text{p,in}}/\Omega = 17.2$, $\omega_{\text{p,out}}/\Omega = 8.6$. In Fig. 6(a), we show a snapshot of the wave component $E_y(x, z)$. We see that a whistler with wavelength $\lambda = 1.2c/\Omega$ propagates within and is guided along the channel. Outside the channel the disturbance is evanescent, as predicted by theory. In Fig. 6(b), the same wave is initiated in a uniform plasma with $\omega_{\text{p}}/\Omega = 17.2$. Since there is no channel the wave fills a cone that expands in x, with a consequent steady drop in amplitude. The simulations also show regimes in which ducting occurs in reduced-density channels, and regimes in which lossy ducting occurs.

9. Summary

We have presented a new hybrid simulation scheme HEMPIC which includes the full nonlinear kinetic phenomena involved in whistler evolution, works in homogeneous or inhomogeneous situations, is not restricted to a single coherent mode, eliminates the speed-of-light time scale and the electron plasma oscillation time scale, and concentrates simulation resources on the parts of the electron distribution that make kinetic contributions to wave growth. The elements of the code are as follows. (1) The plasma is represented as a cold fluid component plus a set of simulation particles. At our option, the simulation particles can be chosen to represent any part of the electron velocity distribution that is of kinetic interest, e.g. the complete ensemble of energetic electrons, or only a set of resonant electrons. (2) Quasineutrality is enforced, i.e., $\nabla \cdot \mathbf{J} = 0$. We emphasize that this does not mean that there are no electrostatic fields, only that $|n_i - n_e| \ll n_i$ and that the electrostatic part of the electric field $\mathbf{E}$ is determined by quasineutrality, rather than by solving Poisson's equation. This assumption is appropriate when the frequencies of interest are slow compared to the plasma frequency, and it eliminates plasma oscillations from the system. In our case, an elliptic equation for $\mathbf{E}$ is derived that combines Faraday's and Ampere's laws, the cold-fluid momentum equation, and a stress tensor constructed from the particle velocities. (3) The displacement current is neglected, since the waves of interest are slow compared to c. This is similar to the Darwin model. However, (1) and (2) allow us to neglect the *full* displacement current, not just the solenoidal part, and thereby avoid all of the complications of the Darwin model. (4) Faraday's and Ampere's laws, rather than a momentum conservation equation, are used to push the cold-fluid velocity. This guarantees quasineutrality. (5) The simulation particles are pushed in standard PIC fashion. (6) The magnetic field is determined by Ampere's law.

In the linear regime, the scheme reproduces the quasi-longitudinal dispersion relation for whistlers, and is accurate for propagation angles up to and beyond the resonance cone. An accurate and extremely stable predictor–corrector–corrector scheme is used to solve the equations. The code need not resolve spatial scales smaller than the wavelengths of interest, nor time scales shorter than the gyrofrequency. As illustrations of the use of the code, we have presented studies of the long-time nonlinear evolution of whistler instabilities, and of whistler ducting in density channels.

References

[1] T.H. Stix, Waves in Plasmas, AIP, New York, 1992.
[2] R.A. Helliwell, Whistlers and Related Ionospheric Phenomena, Stanford University Press, Stanford, CA, 1965.
[3] D.W. Hewett, Comput. Phys. Commun. 84 (1994) 243.
[4] G. DiPeso, D.W. Hewett, G.F. Simonson, J. Comput. Phys. 111 (1994) 237.
[5] D. Nunn, Comput. Phys. Commun. 60 (1990) 1.
[6] Y. Omura, D. Nunn, H. Matsumoto, M.J. Rycroft, J. Atmos. Terr. Phys. 53 (1991) 351.
[7] J.P. Boris, Relativistic plasma simulation – optimization of a hybrid code, in: Proc. Fourth Conf. Num. Sim. Plasmas, Naval Research Laboratory, Washington, DC, 1970, pp. 3–67.
[8] C.K. Birdsall, A.B. Langdon, Plasma Physics via Computer Simulation, McGraw-Hill, New York, 1985, p. 59.
[9] R.A. Helliwell, Rev. Geophys. 26 (1988) 551.

[10] J.L. Vomvoridis, J. Denavit, Phys. Fluids 22 (1979) 367.
[11] J.L. Vomvoridis, J. Denavit, Phys. Fluids 23 (1980) 174.
[12] J.L. Vomvoridis, T.L. Crystal, J. Denavit, J. Geophys. Res. 87 (1982) 1473.
[13] A.G. Demekhov, V.Yu. Trakhtengerts, Radiophysics and Quantum Electronics, Springer, Germany, 2001.
[14] K.R. Chu, J.L. Hirshfield, Phys. Fluids 21 (1978) 461.
[15] P. Palmadesso, G. Schmidt, Phys. Fluids 14 (1971) 1411.
[16] T.M. O'Neil, Phys. Fluids 8 (1965) 2255.
[17] R.A. Helliwell, T.L. Crystal, J. Geophys. Res. 78 (1973) 7357.
[18] R.L. Smith, R.A. Helliwell, I.W. Yabroff, J. Geophys. Res. 65 (1960) 815.
[19] R. Stenzel, Phys. Rev. Lett. 35 (1975) 574.
[20] R. Stenzel, Phys. Fluids 19 (1976) 857.
[21] R. Stenzel, Phys. Fluids 19 (1976) 865.